Journal of Saudi Chemical Society (2018) **22**, 459–468

King Saud University

Journal of Saudi Chemical Society

www.ksu.edu.sa
www.sciencedirect.com

ORIGINAL ARTICLE

Systematic trends in (001) surface *ab initio* calculations of ABO_3 perovskites

R.I. Eglitis *, **A.I. Popov**

Institute of Solid State Physics, University of Latvia, 8 Kengaraga Str., Riga LV1063, Latvia

Received 5 April 2017; revised 18 May 2017; accepted 31 May 2017
Available online 13 June 2017

KEYWORDS

Ab initio calculations;
B3PW;
B3LYP;
ABO_3 perovskites;
(001) surfaces

Abstract By means of the hybrid exchange–correlation functionals, as it is implemented in the CRYSTAL computer code, *ab initio* calculations for main ABO_3 perovskite (001) surfaces, namely $SrTiO_3$, $BaTiO_3$, $PbTiO_3$, $CaTiO_3$, $SrZrO_3$, $BaZrO_3$, $PbZrO_3$ and $CaZrO_3$, were performed. For ABO_3 perovskite (001) surfaces, with a few exceptions, all atoms of the upper surface layer relax inward, all atoms of the second surface layer relax outward, and all third layer atoms, again, inward. The relaxation of (001) surface metal atoms for ABO_3 perovskite upper two surface layers for both AO and BO_2-terminations, in most cases, are considerably larger than that of oxygen atoms, what leads to a considerable rumpling of the outermost plane. The ABO_3 perovskite (001) surface energies always are smaller than the (011) and especially (111) surface energies. The ABO_3 perovskite AO and BO_2-terminated (001) surface band gaps always are reduced with respect to the bulk values. The B–O chemical bond population in ABO_3 perovskite bulk always are smaller than near the (001) and especially (011) surfaces.

1. Introduction

Surface and interface phenomena, occurring in the complex oxide materials and their nanostructures, the nature of surface and interface states, and the mechanisms of surface electronic processes are very important topics in modern solid state physics [1–15]. $SrTiO_3$, $BaTiO_3$, $PbTiO_3$, $CaTiO_3$, $SrZrO_3$, $BaZrO_3$, $PbZrO_3$ and $CaZrO_3$ perovskites belongs to the family of ABO_3-type perovskite oxides, and possess a large number of industrially important applications, including charge storage devices, capacitors, actuators, as well as many others [16–21]. Therefore, it is obvious, that in last quarter of century $SrTiO_3$, $BaTiO_3$, $PbTiO_3$, $CaTiO_3$, $SrZrO_3$, $BaZrO_3$, $PbZrO_3$ and $CaZrO_3$ perovskites and their (001) surfaces were worldwide extensively investigated both theoretically and experimentally [18–47].

Each of these ABO_3 perovskites displays a different sequence of structural phase transitions from the cubic para-electric phase as the temperature is lowered. At room temperature $SrTiO_3$ and $BaZrO_3$ are known to have cubic structures, whereas $CaTiO_3$, $SrZrO_3$, $PbZrO_3$ and $CaZrO_3$ are at orthorhombic structures. On the other hand, $PbTiO_3$ shows tetragonal structure, while $BaTiO_3$ has the tetragonal–orthorhombic phase transition just at temperatures close to

* Corresponding author.
E-mail address: rieglitis@gmail.com (R.I. Eglitis).
Peer review under responsibility of King Saud University.

Production and hosting by Elsevier

http://dx.doi.org/10.1016/j.jscs.2017.05.011

room temperature. The experimental temperature of the transition from the low temperature phase to the high temperature cubic structure, the appropriate experimental lattice parameters as well as experimentally evaluated band gap energies E_g [48–68] are reviewed in Table 1. Note here that in most cases the experimental band gap energy values are obtained at room temperatures (RT) and in a few cases between 4.2 K and RT, while for most of the high temperature cubic modifications due to the technical impossibility to perform optical measurements, the appropriate experimental data are not available. It is worth to notice, that for $BaTiO_3$ perovskite no uniquely defined band gap can be detected from an exponential edge, Wemple proposes [50], using as a basis indirect arguments, that the room temperature band gaps are equal to 3.38 and 3.27 eV, respectively, for light polarized parallel and perpendicular to the ferroelectric ***c*** axis (Table 1).

Caused by explosive development of new and emerging technologies, the atomic and electronic properties as well as the structure of the ABO_3 perovskite (0 0 1) surfaces have been intensively explored experimentally during the last years. For example, the $SrTiO_3$ (0 0 1) surface structure has been experimentally analyzed by means of the atomic force microscopy [39], transmission electron microscopy (TEM) [40], low-energy electron diffraction and scanning tunneling microscopy [41], scanning probe microscopy [42] as well as high resolution X-ray photoelectron spectroscopy (XPS) [43]. Ultraviolet Photoelectron Spectroscopy (UPS) studies were performed on $BaTiO_3$ (0 0 1) surfaces [44]. Microscopic structure and electronic states on the (0 0 1) $BaTiO_3$ single-crystal surfaces annealed in ultrahigh vacuum were observed by scanning tunneling microscopy and spectroscopy (STM/S) [45]. Nevertheless, it is worth to notice, that for the SrO-terminated $SrTiO_3$ (0 0 1) surface, the low energy electron diffraction (LEED) [46] and reflection high-energy electron diffraction (RHEED) [47] experiments clearly contradict each other regarding the compression or extension of the interlayer distance Δd_{12}, probably because of differences in sample preparation or different interpretations of indirect experimental data on the atomic surface relaxations.

On the theory side, it is much more easy to calculate the ABO_3 perovskite (0 0 1) surface, which is neutral, than the very complex polar and charged (0 1 1) or (1 1 1) surfaces [69–73]. In this paper, the comprehensive *ab initio* calculations dealing with $SrTiO_3$, $BaTiO_3$, $PbTiO_3$, $CaTiO_3$, $SrZrO_3$, $BaZrO_3$, $PbZrO_3$ and $CaZrO_3$ (0 0 1) surfaces focusing on surface relaxations, chemical bond covalencies, optical band gaps and surface energies were performed and obtained systematic trends, common for all eight perovskites, were analyzed.

For example, experimentally detected Γ–Γ band gap for the $SrTiO_3$ bulk in the cubic phase is equal to 3.75 eV [49], whereas no experimental data exist for the band gap at $BaTiO_3$ cubic phase. The direct $BaTiO_3$ band gap detected in the tetragonal to orthorhombic phase transition temperature 278 K at different experimental conditions is equal to 3.27 or 3.38 eV [50]. It is well known that the Hartree–Fock (HF) method systematically overestimates the band gap of solids. Indeed, our by means of the HF method calculated Γ–Γ band gaps for $SrTiO_3$ and $BaTiO_3$ are equal to 12.33 and 11.73 eV, respectively [74]. From another side, the Density Functional Theory (DFT), as a rule, strongly underestimate the band gap of solids. For example, the LDA calculated Γ–Γ band gaps for $SrTiO_3$ and $BaTiO_3$ are equal to 2.36 and 1.98 eV, respectively [74]. In order to get a reliable basis for further ABO_3 perovskite bulk and (0 0 1) surface defect calculations, which requires a precise description of the optical band gap, we performed most of our calculations by means of the hybrid exchange–correlation functionals B3PW and B3LYP, which coinjoin 20% of the HF and 80% of the DFT Hamiltonian, as it is implemented in the CRYSTAL computer code. Logically, that the hybrid exchange–correlation functionals, since they are a combination of HF and DFT Hamiltonians, allows to achieve a fair agreement between *ab initio* calculated and experimentally measured band gaps for ABO_3 perovskite bulk as well as their (0 0 1) surfaces.

Table 1 Experimental data for ABO_3 perovskites, including band gap values (in eV) and lattice constants (in Å).

Material	Structure at RT	Band gap E_g (eV) at RT	Transition Temp. to cubic phase (K)	Expt. lattice const. (Å) in cubic phase
$SrTiO_3$	Cubic	3.75 eV (direct); 3.25 eV (indirect) .25 eV (indirect) [49]	110 K [58]	3.89845 Å–110 K [55] 3.9053 Å–293 K [51]
$BaTiO_3$	Tetragonal ↔ orthorhombic (278 K)	3.38 eV (// ***c***); 3.27 eV (⊥ ***c***) [50]	403 K [58]	4.0037 Å–474 K [48] 4.0136 Å–674 K [48] 4.0239 Å–874 K [48] 4.0415 Å–1174 K [48] 4.0539 Å–1387 K [48] 4.0658 Å–1574 K [48] 4.0701 Å–1645 K [48]
$PbTiO_3$	Tetragonal	3.4 eV [60,66]	763 K [54] 763 K [52]	3.970 Å–777 K [52]
$CaTiO_3$	Orthorhombic	∼3.5 eV [67]	1647 K [62]	3.8967 Å–777 K [62]
$SrZrO_3$	Orthorhombic	5.6 eV [68]	1433 K [63] 1360 K [59]	4.154 Å–1423 K [59]
$BaZrO_3$	Cubic	5.3 eV [60]	Cubic in all T	4.199 Å–RT [56]
$PbZrO_3$	Orthorhombic	3.7 eV [60]	501–508 K [53]	4.1614 Å–520 K [61]
$CaZrO_3$	Orthorhombic	5.7 eV [65]	2173 ± 100 K [57,64]	No data for cubic phase

The goal of work reported here was to perform necessary additional calculations in order to complete our more than fifteen year long work dealing with theoretical investigations of ABO_3 perovskite (0 0 1) surfaces. After completing *ab initio* calculations for $SrTiO_3$, $BaTiO_3$, $PbTiO_3$, $CaTiO_3$, $SrZrO_3$, $BaZrO_3$, $PbZrO_3$ and $CaZrO_3$ perovskites, the results were analyzed and systematic trends common for all eight ABO_3 perovskites were detected and systematized in a form easily accessible for a broad audience of readers.

2. Calculation details for the ABO_3 perovskite (0 0 1) surfaces

Comparative *ab initio* calculations, using the hybrid exchange–correlation functionals B3PW [75] or B3LYP [76] and the CRYSTAL computer code [77], have been carried out in this paper for the eight most important ABO_3 perovskite (0 0 1) surfaces. The reciprocal-space integration, in most cases, were performed by sampling the Brillouin zone with an $8 \times 8 \times 8$ times extended Pack–Monkhorst net [78]. Strength of the CRYSTAL computer code is that it allows to calculate isolated two-dimensional slabs perpendicular to the crystal surface, without any artificial periodicity in the z direction.

With aim to calculate ABO_3 perovskite (0 0 1) surfaces, symmetrical slabs consisting of nine alternating AO and BO_2 layers were used. First slab was terminated by AO planes and consisted of a supercell which contained 22 atoms (Fig. 1). Another slab from both sides was terminated by BO_2 planes and thereby consisted of a supercell containing 23 atoms (Fig. 2). Both slabs were non-stoichiometric, with following unit cell equations $A_5B_4O_{13}$ and $A_4B_5O_{14}$, respectively.

First step, in order to calculate the energy for ABO_3 perovskite (0 0 1) surface is the cleavage energy calculations for unrelaxed AO and BO_2-terminated (0 0 1) surfaces. The cleavage energy is equally distributed between the created surfaces, as a result of simultaneous (0 0 1) cleavage of the crystal. In

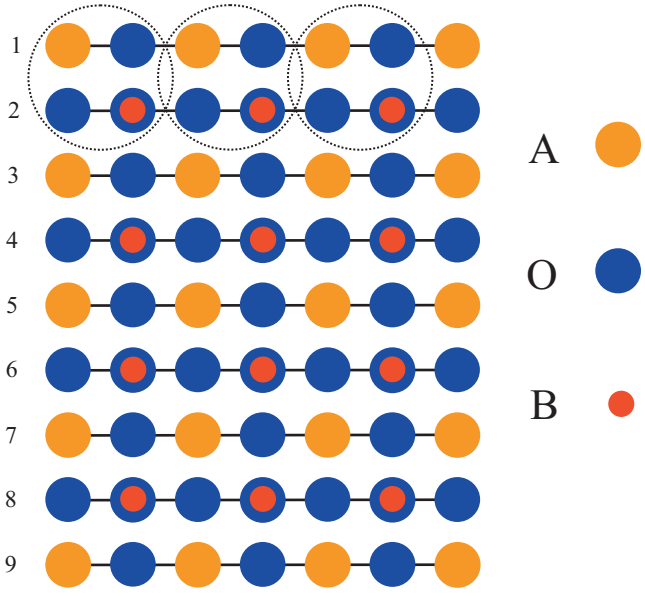

Fig. 1 Side view of the AO-terminated ABO_3 perovskite (0 0 1) surface which contains 9 layers.

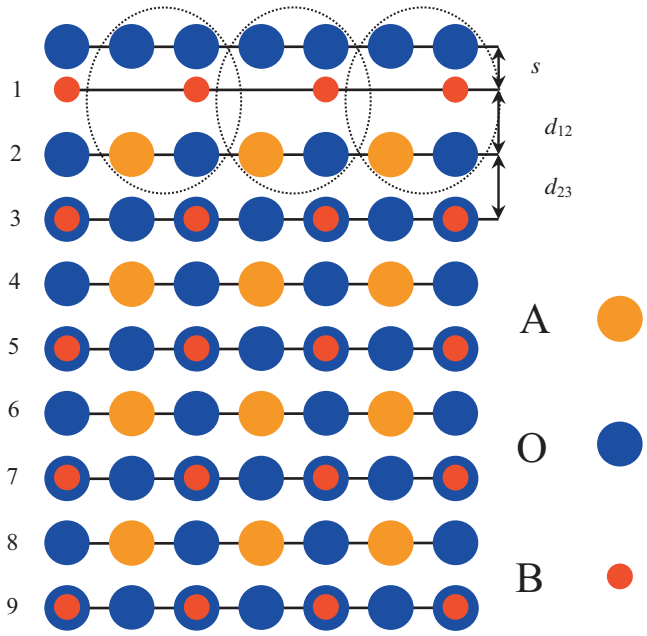

Fig. 2 Side view of the BO_2-terminated ABO_3 perovskite (0 0 1) surface containing the definitions of the surface rumpling and the near-surface interplane distances.

performed calculations, the nine-layer AO-terminated (0 0 1) slab with 22 atoms and BO_2-terminated slab, containing 23 atoms, represent together nine bulk unit cells, or in another words 45 atoms:

$$E^{unr}_{surf}(\zeta) = \frac{1}{4}\left[E^{unr}_{slab}(AO) + E^{unr}_{slab}(BO_2) - 9E_{bulk}\right],$$

where ζ means AO or BO_2. $E^{\mathrm{unr}}_{\mathrm{surf}}(\zeta)$ are the total energies for the unrelaxed AO or BO_2-terminated ABO_3 (0 0 1) slabs. E_{bulk} is the total energy per bulk unit cell. The factor of ¼ comes as a consequence from the fact that four surfaces have been created upon the crystal cleavage procedure. As a next step, the relaxation energies for each of AO and BO_2-terminations were calculated, when both sides of the slabs relax, as follows:

$$E_{rel}(\zeta) = \frac{1}{2}\left[E^{rel}_{slab}(\zeta) - E^{unr}_{slab}(\zeta)\right],$$

where $E^{\mathrm{rel}}_{\mathrm{slab}}(\zeta)$ is the slab energy after the geometry relaxation. Finally, the surface energy may be calculated as follows:

$$E_{surf}(\zeta) = E^{unr}_{surf}(\zeta) + E_{rel}(\zeta).$$

In order to describe the chemical bonding and covalency effects for both ABO_3 perovskite bulk and their (0 0 1) surfaces, we employed a standard Mulliken population analysis for the effective atomic charges q, chemical bond populations P and other local properties of electronic structure, for example, bond orders, atomic covalencies as well as full valencies [77,79]. Our calculated ABO_3 perovskite (0 0 1) and (0 1 1) surface B–O chemical bond populations are detected for fully relaxed, final surface structures.

In our ABO_3 perovskite (0 0 1) surface structure calculations we allowed all atoms of the three outermost surface layers to relax only the in direction along the z-axis, since surfaces of perfect cubic perovskite crystals by symmetry have no forces acting along the x- and y-axes. Our calculated ABO_3

perovskite (0 0 1) surface BO_2 layers contain two by symmetry equivalent oxygen atoms, which both exhibit completely equal relaxation magnitudes and directions. We reported in tables the relaxation values only for one oxygen atom, but the relaxation parameters for the second oxygen are exactly the same.

3. Calculation results for (0 0 1) surfaces by means of B3PW or B3LYP functionals

As a starting point of our B3PW and B3LYP calculations, the theoretical bulk lattice constants were calculated for $SrTiO_3$, $BaTiO_3$, $PbTiO_3$, $CaTiO_3$, $SrZrO_3$, $BaZrO_3$, $PbZrO_3$ and $CaZrO_3$ perovskites [18–20,29,32,38,69,73,74] and compared with the available experimental data [52,56,59,61,62,80] (Tables 1 and 2). As we can see from Table 2, the B3PW calculated $BaTiO_3$ bulk lattice constant (4.008 Å) only by 0.2% overestimate the experimental value of (4.00 Å) [80]. Our B3PW and B3LYP calculations gives exactly the same result for $BaZrO_3$ bulk lattice constant 4.234 Å. Thereby our B3PW and B3LYP calculated $BaZrO_3$ bulk lattice constant (4.234 Å) is only by 0.83% overestimated with respect to the experimental value of 4.199 Å [56].

It is interesting to notice that our B3LYP calculated bulk lattice constants for all $AZrO_3$ (A = Ca; Sr; Pb; Ba) perovskites (4.157 Å; 4.195 Å; 4.220 Å; 4.234 Å) are always larger than for $ATiO_3$ perovskites (3.851 Å; 3.94 Å; 3.96 Å; 4.04 Å) (Table 2). Moreover, for both $AZrO_3$ and $ATiO_3$ perovskites, the B3LYP calculated bulk lattice constants increases exactly in the same order as a function from A (A = Ca; Sr; Pb and Ba). In Figs. 3, 4, 5 and 6 on the *x* axis we ordered all eight perovskites ($CaTiO_3$; $SrTiO_3$; $PbTiO_3$; $BaTiO_3$; $CaZrO_3$; $SrZrO_3$; $PbZrO_3$ and $BaZrO_3$) in direction of increase in our B3LYP calculated bulk lattice constants (3.851 Å; 3.94 Å; 3.96 Å; 4.04 Å; 4.157 Å; 4.195 Å; 4.220 Å; 4.234 Å),

Table 2 B3PW, B3LYP, PWGGA and HF calculated bulk lattice constants (in Å) for the $SrTiO_3$, $BaTiO_3$, $PbTiO_3$, $CaTiO_3$, $SrZrO_3$, $BaZrO_3$, $PbZrO_3$ and $CaZrO_3$ bulk. The experimental results are listed for comparison purpose.

Material	Functional	Theory	Experiment
$SrTiO_3$	B3PW	3.904 [20]	3.89 [80]
	B3LYP	3.94 [74]	
$BaTiO_3$	B3PW	4.008 [19]	4.00 [80]
	B3LYP	4.04 [74]	
$PbTiO_3$	B3PW	3.936 [19]	3.97 [52]
	B3LYP	3.96 [74]	
$CaTiO_3$	B3PW	3.851 [18]	3.8967 [62]
	B3LYP	3.851 [73]	
	PWGGA	3.884	
	HF	3.863	
$SrZrO_3$	B3PW	4.155	4.154 [59]
	B3LYP	4.195 [29]	
	GGA	4.176	
	HF	4.182	
$BaZrO_3$	B3PW	4.234 [32]	4.199 [56]
	B3LYP	4.234 [69]	
	PWGGA	4.240	
	HF	4.250	
$PbZrO_3$	B3LYP	4.220 [29]	4.1614 [61]
$CaZrO_3$	B3LYP	4.157 [38]	No data for cubic phase

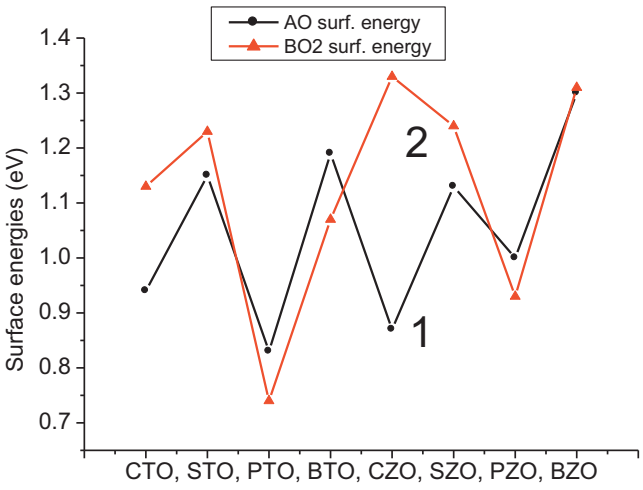

Fig. 3 Calculated surface energies for AO-terminated (1) and BO_2-terminated (2) (0 0 1) surfaces of $CaTiO_3$ (CTO), $SrTiO_3$ (STO), $PbTiO_3$ (PTO), $BaTiO_3$ (BTO), $CaZrO_3$ (CZO), $SrZrO_3$ (SZO), $PbZrO_3$ (PZO) and $CaZrO_3$ (CZO) perovskites by means of the hybrid B3PW or B3LYP exchange–correlation functionals.

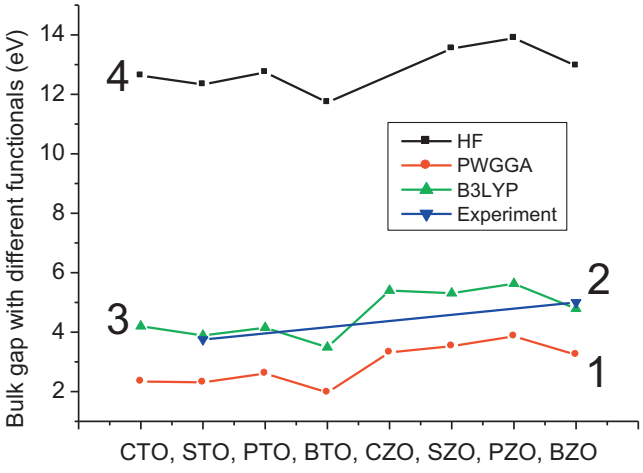

Fig. 4 Calculated and experimental bulk Γ–Γ band gaps for eight ABO_3 perovskites obtained by means of different exchange–correlation functionals: (1) PWGGA; (2) Experiment; (3) B3LYP; (4) HF.

respectively. It is worth to notice, that the increase in our B3LYP calculated ABO_3 perovskite bulk lattice constants in direction from $CaTiO_3$ to $BaZrO_3$ may be explained with an increase in ionic radiuses of divalent metallic ions in the same direction Ca^{+2} (0.99 Å); Sr^{+2} (1.12 Å); Pb^{+2} (1.20 Å) and Ba^{+2} (1.34 Å). The ionic radius for tetravalent Zr^{+4} (0.79 Å) is larger than for Ti^{+4} (0.68 Å) [81].

B3PW and B3LYP calculation results for the surface atomic relaxations for AO and BO_2-terminated $SrTiO_3$, $BaTiO_3$, $PbTiO_3$, $CaTiO_3$, $SrZrO_3$, $BaZrO_3$, $PbZrO_3$ and $CaZrO_3$ material upper two or three (0 0 1) surface layers are listed in Tables 3 and 4. As we can see from Tables 3 and 4, the relaxation of surface metal atoms for ABO_3 perovskite upper two surface layers for both (0 0 1) terminations—AO and BO_2, in most cases, are considerably larger than that of

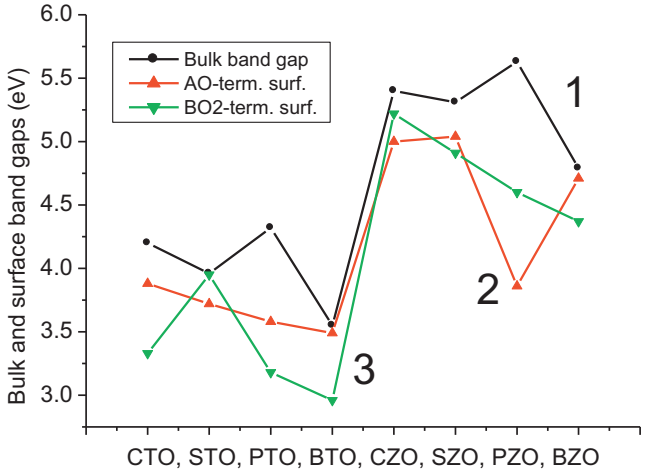

Fig. 5 Calculated bulk (1) as well as AO (2) and BO_2-terminated (3) (001) surface Γ–Γ band gaps for eight ABO_3 perovskites using B3PW or B3LYP hybrid exchange–correlation functionals.

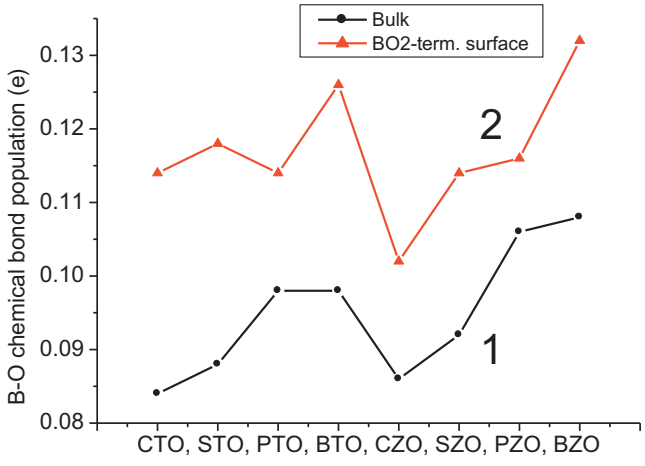

Fig. 6 Calculated bulk (1) and BO_2-terminated (2) (001) surface B–O chemical bond populations for eight ABO_3 perovskites using B3PW or B3LYP hybrid exchange–correlation functionals.

oxygen atoms (Tables 3 and 4), what leads to a considerable rumpling of the outermost plane (Table 5). The only two exceptions are the ZrO_2-terminated $SrZrO_3$ and $CaZrO_3$ perovskite (001) surface upper layers, where the Sr and Ca metal atom relaxations are smaller, than the oxygen atom relaxations. For the AO and ZrO_2-terminated (001) surfaces of ABO_3 perovskites, the systematic trend, according to performed B3PW and B3LYP calculations, is that all atoms of the first surface layer relax inward, all atoms of the second surface layer relax outward, and all atoms of the third surface layer, again, relax inward. The only exceptions are SrO-terminated $SrTiO_3$ (001) surface first, and $SrZrO_3$ (001) surface second layer, respectively, oxygen atoms, which relax in opposite directions, as well as TiO_2-terminated $PbTiO_3$ (001) surface upper layer oxygen atom (Tables 3 and 4). It is worth to notice, that the ZrO_2-terminated $BaZrO_3$ (001) surface third layer oxygen atom displacement is already negligible, namely close to zero (0.00), and it is impossible, according to performed B3PW calculations, to detect the displacement direction for this atom (Table 4). According to performed B3LYP calculations, the CaO-terminated $CaZrO_3$ (001) surface upper layer Ca atom exhibit the strongest relaxation between all calculated AO and BO_2-terminated ABO_3 perovskite (001) surface atoms. The Ca atom inward relaxation magnitude exceeds ten percent of the lattice constant, and according to performed B3LYP calculations is equal to 10.01%.

With an aim to compare experimental results with our B3PW and B3LYP calculated (001) surface structures, the surface rumpling s (the relative displacement of oxygen atom regarding to the metal atom in the upper surface layer) and the changes in interlayer distances Δd_{12} and Δd_{23} are listed in Table 5. The surface rumpling and interlayer distances were calculated for fully relaxed ABO_3 perovskite (001) surfaces, where all atoms are located at the energy minimum positions. For *ab initio* calculations of the interlayer distances we used the positions of relaxed metal atoms, which are much stronger electron scatterers than oxygen atoms [46]. Our B3PW calculations for $SrTiO_3$ (001) surfaces [20] are in a good agreement with previous LDA calculations performed by Meyer et al. [58], which give the same sign for changes of the interlayer distances. Our calculated surface rumpling amplitudes s for SrO and TiO_2-terminated $SrTiO_3$ (001) surfaces are in a qualitative agreement with the existing LEED [46] and RHEED [47] experiments. Nevertheless, the calculated interlayer distance changes disagree with the LEED experiments for the TiO_2-terminated $SrTiO_3$ (001) surface. At the same time both LEED and RHEED experiments (Table 5) contradict each other regarding the sign of Δd_{12} for the SrO-terminated $SrTiO_3$

Table 3 Our B3PW and B3LYP calculated relaxation of atoms (in percent of bulk lattice constant) for SrO, BaO, PbO and CaO-terminated $SrTiO_3$, $BaTiO_3$, $PbTiO_3$, $CaTiO_3$, $SrZrO_3$, $BaZrO_3$, $PbZrO_3$ and $CaZrO_3$ (001) surfaces totally came from references [18–20,29,32,38]. Positive (negative) values refer to displacements outward from (inward to) the surface.

Material		$SrTiO_3$	$BaTiO_3$	$PbTiO_3$	$CaTiO_3$	$SrZrO_3$	$BaZrO_3$	$PbZrO_3$	$CaZrO_3$
(001)-termination		SrO	BaO	PbO	CaO	SrO	BaO	PbO	CaO
Layer	Ion	B3PW	B3PW	B3PW	B3PW	B3LYP	B3PW	B3LYP	B3LYP
1	A	−4.84	−1.99	−3.82	−8.31	−7.63	−4.30	−5.69	−10.01
	O	0.84	−0.63	−0.31	−0.42	−0.86	−1.23	−2.37	−0.79
2	B	1.75	1.74	3.07	1.12	0.86	0.47	0.57	1.11
	O	0.77	1.40	2.30	0.01	−0.05	0.18	0.09	0.01
3	A	–	–	–	–	−1.53	−0.01	−0.47	−2.60
	O	–	–	–	–	−0.45	−0.14	−0.47	−0.48

Table 4 Our B3PW and B3LYP calculated atomic relaxation for BO_2-terminated $SrTiO_3$, $BaTiO_3$, $PbTiO_3$, $CaTiO_3$, $SrZrO_3$, $BaZrO_3$, $PbZrO_3$ and $CaZrO_3$ (001) surfaces totally came from references [18–20,29,32,38].

Material		$SrTiO_3$	$BaTiO_3$	$PbTiO_3$	$CaTiO_3$	$SrZrO_3$	$BaZrO_3$	$PbZrO_3$	$CaZrO_3$
(001)-termination		TiO_2	TiO_2	TiO_2	TiO_2	ZrO_2	ZrO_2	ZrO_2	ZrO_2
Layer	Ion	B3PW	B3PW	B3PW	B3PW	B3LYP	B3PW	B3LYP	B3LYP
1	B	−2.25	−3.08	−2.81	−1.71	−1.38	−1.79	−2.37	−1.30
	O	−0.13	−0.35	0.31	−0.10	−2.10	−1.70	−1.99	−2.31
2	A	3.55	2.51	5.32	2.75	2.81	1.94	4.36	4.23
	O	0.57	0.38	1.28	1.05	0.91	0.85	1.04	1.25
3	B	–	–	–	–	−0.04	−0.03	−0.47	−0.05
	O	–	–	–	–	−0.05	0.00	−0.28	−0.09

Table 5 B3PW and B3LYP calculated and experimentally measured surface rumpling s and relative displacements Δd_{ij} (in percent of the bulk lattice constant) of the three near-surface planes for the AO and BO_2-terminated $SrTiO_3$, $BaTiO_3$, $PbTiO_3$, $CaTiO_3$, $SrZrO_3$, $BaZrO_3$, $PbZrO_3$ and $CaZrO_3$ (001) surfaces [18–20,29,32,38,46,47]. LDA and GGA calculation results of other authors from Refs. [58,82,83] are listed for comparison purposes.

Material	Method	AO-terminated			BO_2-terminated		
		s	Δd_{12}	Δd_{23}	s	Δd_{12}	Δd_{23}
$SrTiO_3$	B3PW [20]	5.66	−6.58	1.75	2.12	−5.79	3.55
	LDA [58]		−3.4	1.2		−3.5	1.6
	LEED [46]	4.1 ± 2	−5 ± 1	2 ± 1	2.1 ± 2	1 ± 1	−1 ± 1
	RHEED [47]	4.1	2.6	1.3	2.6	1.8	1.3
$BaTiO_3$	B3PW	1.37	−3.74	1.74	2.73	−5.59	2.51
	LDA [58]		−2.8	1.1		−3.1	0.9
$PbTiO_3$	B3PW	3.51	6.89	3.07	3.12	−8.13	5.32
	LDA [58]		−4.2	2.6		−4.4	3.1
$CaTiO_3$	B3PW	7.89	−9.43	1.12	1.61	−4.46	2.75
	GGA [82]	0.37	−0.44	0.22	0.13	−0.41	0.33
$SrZrO_3$	B3LYP	6.77	−8.49	2.39	−0.72	−4.19	2.85
	LDA [83]	7.9	−9.1	3.2	−0.7	−6.1	4.2
	GGA [83]	7.8	−9.3	3.3	0.3	−7.4	4.9
$BaZrO_3$	B3PW	3.07	−4.77	0.48	0.09	−3.73	1.97
$PbZrO_3$	B3LYP	3.32	−6.26	1.04	0.38	−6.73	4.83
$CaZrO_3$	B3LYP	9.22	−11.12	3.71	1.01	−5.53	4.28

(001) surface, as well as for Δd_{23} on the TiO_2-terminated (001) surface. LDA and GGA calculation results for $CaTiO_3$ and $SrZrO_3$ perovskites from Refs. [82,83] are listed in Table 5 for comparison purposes. As follows from our performed B3PW calculations, the amplitude of surface rumpling for SrO-terminated $SrTiO_3$ (001) surface is considerably larger than that for TiO_2-terminated $SrTiO_3$ (001) surface. Just opposite, the rumpling of $BaTiO_3$ TiO_2-terminated (001) surface, according to performed B3PW calculations, exceeds the surface rumpling for BaO-terminated $BaTiO_3$ (001) surface by a factor of two. The B3PW calculated surface rumpling for PbO-terminated $PbTiO_3$ (001) surface (3.51) is rather close to the TiO_2-terminated $PbTiO_3$ (001) surface rumpling (3.12). Two largest surface rumplings, among all eight calculated ABO_3 perovskites for AO and BO_2-terminated (001) surfaces, are B3LYP calculated surface rumpling for $CaZrO_3$ CaO-terminated (001) surface (9.22), and B3PW calculated surface rumpling for $CaTiO_3$ CaO-terminated (001) surface (7.89). It is interesting to notice, that among all eight calculated ABO_3 perovskites, there are only two almost perfectly coinciding negative surface rumplings, namely, for ZrO_2-terminated $SrZrO_3$ (001) surface (−0.72) obtained in our B3LYP calculations [29] as well as (−0.7) according to LDA calculations performed by Wang et al. [83].

As we can see from Table 5, for both terminations of all eight calculated perovskites, all our B3PW and B3LYP calculated surfaces exhibit the reduction of the interlayer distance Δd_{12} and expansion of Δd_{23}. The single exception from this general trend in our calculations is the $PbTiO_3$ PbO-terminated (001) surface, where the expansion between the first and second surface layer equal to 6.89% of a_0 was observed. Nevertheless, it is worth to notice, that the LDA calculations performed in the Ref. [58] are in a line with the systematic trend and yields the reduction of the interlayer distance Δd_{12} for the PbO-terminated $PbTiO_3$ (001) surface by 4.2% of a_0. For all eight B3PW and B3LYP calculated ABO_3 perovskites, the changes in interlayer distances Δd_{12} are larger than the respective changes in the interlayer distances Δd_{23}.

The largest reduction of the interlayer distance Δd_{12} between all eight calculated ABO_3 perovskites is observed for CaO-terminated $CaZrO_3$ (0 0 1) surface (−11.12), whereas the largest expansion of the interlayer distance Δd_{23} is observed for TiO_2-terminated $PbTiO_3$ (0 0 1) surface (5.32).

According to our performed B3PW calculations (Table 6 and Fig. 3), the surface energy for the CaO-terminated $CaTiO_3$ (0 0 1) surface is 0.94 eV, which is by 0.19 eV smaller than the calculated surface energy of 1.13 eV for the TiO_2-terminated $CaTiO_3$ (0 0 1) surface [18]. In contrast to the ABO_3 perovskite (0 0 1) surfaces, the different terminations of the (0 1 1) and especially (1 1 1) surfaces lead to a huge differences in the surface energies. According to performed B3PW calculations for the $CaTiO_3$ (0 1 1) surface, the lowest surface energy is 1.86 eV for the O-terminated (0 1 1) surface. The B3PW calculated surface energy for the TiO-terminated $CaTiO_3$ (0 1 1) surface (3.13 eV) is considerably larger than the calculated surface energy for Ca-terminated $CaTiO_3$ (0 1 1) surface (1.91 eV) [18]. Nevertheless, the largest $CaTiO_3$ surface energies are for the $CaTiO_3$ (1 1 1) surfaces [73]. They are much larger, than the $CaTiO_3$ (0 0 1), and even $CaTiO_3$ (0 1 1) surface energies. So, the B3LYP calculated CaO_3-terminated $CaTiO_3$ (1 1 1) surface energy is equal to 5.86 eV, but the Ti-terminated $CaTiO_3$ (1 1 1) surface energy is 4.18 eV.

Similar surface energy trends, according to our performed B3PW and B3LYP calculations, are observed also for another ABO_3 perovskites. For example, $BaZrO_3$ (0 0 1) surface energies almost coincide [32]. They are, according to performed B3PW calculations, 1.30 eV for the BaO-terminated $BaZrO_3$ (0 0 1) surface, and 1.31 eV for the ZrO_2-terminated $BaZrO_3$ (0 0 1) surface. Again, $BaZrO_3$ (0 1 1) surface energies are much larger than the (0 0 1) surface energies, similar as for another ABO_3 perovskites. The B3PW calculated O-terminated $BaZrO_3$ (0 1 1) surface energy 2.32 eV is the lowest surface energy between all $BaZrO_3$ (0 1 1) surface energies. The ZrO-terminated $BaZrO_3$ (0 1 1) surface energy 3.09 eV is larger than the Ba-terminated (0 1 1) surface energy 2.90 eV. Again, the B3LYP calculated $BaZrO_3$ (1 1 1) surface energies are considerably larger, than even the BaZrO3 (0 1 1) surface energies [69]. They are equal to 9.33 eV for the BaO_3-terminated $BaZrO_3$ (1 1 1) surface and 7.94 eV for the Zr-terminated $BaZrO_3$ (1 1 1) surface.

Our B3PW and B3LYP calculated bulk optical band gaps [18–20,29,32,38,69,73] for ABO_3 perovskites, as a rule, are in a better agreement with the experimental values [49,60] than the Hartree–Fock or Density Functional Theory calculation results (Table 7 and Fig. 4). For example, the $BaZrO_3$ bulk optical Γ–Γ band gap calculated by us using the B3PW exchange–correlation functional (4.93 eV) is in almost perfect agreement with the experimental value of 5.3 eV [60] (Fig. 7). Our B3PW calculated electronic band structures for BaO and ZrO_2-terminated $BaZrO_3$ (0 0 1) surfaces are graphically depicted in Fig. 8. Our B3PW calculated optical BaO-terminated $BaZrO_3$ (0 0 1) surface Γ–Γ band gap is equal to 4.82 eV, whereas ZrO_2-terminated (0 0 1) surface Γ–Γ band gap is even more reduced with respect to the $BaZrO_3$ bulk band gap value and is equal to 4.48 eV. From Fig. 7 for the $BaZrO_3$ bulk case we can see that the bottom of the lowest conduction band (CB) lies at the Γ-point with quite flat fragment between the Γ and X points and consist of Zr-4d sates. The highest valence band (VB) for the $BaZrO_3$ bulk is relatively flat, with the top at R point and also flat between M and R points (Fig. 7). The VB top in the $BaZrO_3$ bulk consists mainly of O2p atomic orbitals. As we can see from Fig. 8a, the top of the VB for the BaO-terminated $BaZrO_3$ (0 0 1) surface is quite flat throughout the Brillouin zone. The O-2p electronic states make a major contribution to the VB top, while the CB bottom is mostly composed from Zr-4d and Ba-6 s electronic states. Finally, as we can see from Fig. 8b, our B3PW calculated band structure for ZrO_2-terminated $BaZrO_3$ (0 0 1) surface has not so flat VB top, as that for the BaO-terminated (0 0 1) surface. The VB top for the ZrO_2-terminated $BaZrO_3$ (0 0 1) surface is located at the M point. The VB top consists mostly from O-2p electronic states, while the CB bottom mainly is composed of Zr-4d electronic states. For all B3PW and B3LYP calculated ABO_3 perovskites their AO and BO_2-terminated (0 0 1) surface optical band gaps are reduced with respect to the bulk optical band gap values (Table 7 and Fig. 5). It is worth to notice that for $SrTiO_3$, $PbZrO_3$ and $CaZrO_3$ perovskites their AO-terminated (0 0 1) surface optical band gaps are smaller, than the BO_2-terminated (0 0 1) surface optical band gaps. Just opposite, for $CaTiO_3$, $BaTiO_3$, $PbTiO_3$, $SrZrO_3$ and $BaZrO_3$ perovskites their BO_2-terminated (0 0 1) surface optical band gaps are smaller than the AO-terminated (0 0 1) surface optical band gaps.

B3PW and B3LYP calculated B–O chemical bond populations for ABO_3 perovskite bulk are in the range from 0.084*e* for the $CaTiO_3$ bulk case to 0.108*e* for the $BaZrO_3$ bulk (Table 8 and Fig. 6). It is worth to notice, that the Ti-O chemical bond populations for the $BaTiO_3$ and $PbTiO_3$ perovskite bulk coincide and both population values are equal to

Table 6 Our B3PW and B3LYP calculated surface energies (in eV per surface cell) for $SrTiO_3$, $BaTiO_3$, $PbTiO_3$, $CaTiO_3$, $SrZrO_3$, $BaZrO_3$, $PbZrO_3$ and $CaZrO_3$ (0 0 1), (0 1 1) and (1 1 1) surfaces.

Material	(0 0 1) surface		(0 1 1) surface			(1 1 1) surface	
Terminat.	AO	BO_2	BO	A	O	AO_3	B
$SrTiO_3$	1.15 [20]	1.23 [20]	3.06 [20]	2.66 [20]	2.04 [20]	6.30 [73]	4.99 [73]
$BaTiO_3$	1.19 [19]	1.07 [19]	2.04 [19]	3.24 [19]	1.72 [19]	8.40 [71]	7.28 [71]
$PbTiO_3$	0.83 [19]	0.74 [19]	1.36 [19]	2.03 [19]	1.72 [19]	8.11 [71]	6.14 [71]
$CaTiO_3$	0.94 [18]	1.13 [18]	3.13 [18]	1.91 [18]	1.86 [18]	5.86 [73]	4.18 [73]
$SrZrO_3$	1.13 [29]	1.24 [29]	3.61 [29]	2.21 [29]	2.23 [29]	9.45 [71]	7.98 [71]
$BaZrO_3$	1.30 [32]	1.31 [32]	3.09 [32]	2.90 [32]	2.32 [32]	9.33 [69]	7.94 [69]
$PbZrO_3$	1.00 [29]	0.93 [29]	1.89 [29]	1.74 [29]	1.85 [29]	8.21 [71]	6.93 [71]
$CaZrO_3$	0.87 [38]	1.33 [38]					

Table 7 Our B3PW, B3LYP, PWGGA and HF calculated optical band gaps for $SrTiO_3$, $BaTiO_3$, $PbTiO_3$, $CaTiO_3$, $SrZrO_3$, $BaZrO_3$, $PbZrO_3$ and $CaZrO_3$ bulk as well as for AO and BO_2-terminated (001) surfaces. Experimental bulk band gap values are listed for comparison purpose.

Material	Method	Band gap			
		Bulk	Experiment	AO-term. (001)	BO_2-term. (001)
$SrTiO_3$	B3PW [74]	3.96	3.75 [49]	3.72	3.95
$BaTiO_3$	B3PW [74]	3.55	No data for cubic phase	3.49	2.96
$PbTiO_3$	B3PW [74]	4.32	No data for cubic phase	3.58	3.18
$CaTiO_3$	B3PW	4.18	No data for cubic phase	3.87	3.30
	B3LYP	4.20 [73]		3.88	3.33
	PWGGA	2.34		2.19	2.06
	HF	12.63		12.53	11.86
$SrZrO_3$	B3PW	5.30	No data for cubic phase	5.01	4.98
	B3LYP [29]	5.31		5.04	4.91
	PWGGA	3.53		3.20	3.17
	HF	13.54		13.25	13.19
$BaZrO_3$	B3PW	4.93	5.3 [60]	4.82	4.48
	B3LYP	4.79 [69]		4.71	4.37
	PWGGA	3.24		3.08	2.76
	HF	12.96		12.84	12.62
$PbZrO_3$	B3LYP	5.63 [29]	No data for cubic phase	3.86	4.60
$CaZrO_3$	B3LYP	5.40 [38]	No data for cubic phase	5.00	5.22

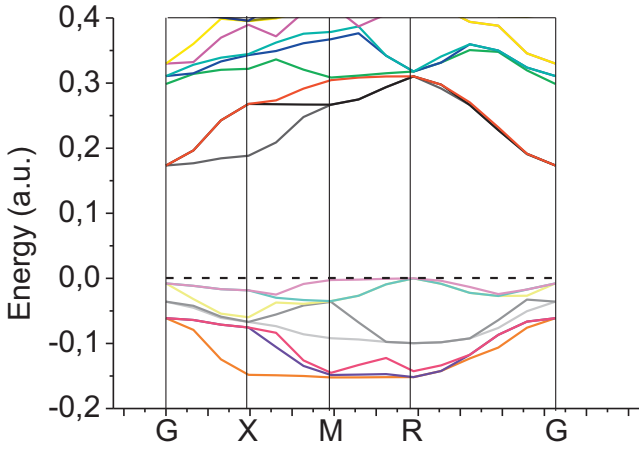

Fig. 7 Our B3PW calculated electronic band structure for $BaZrO_3$ bulk.

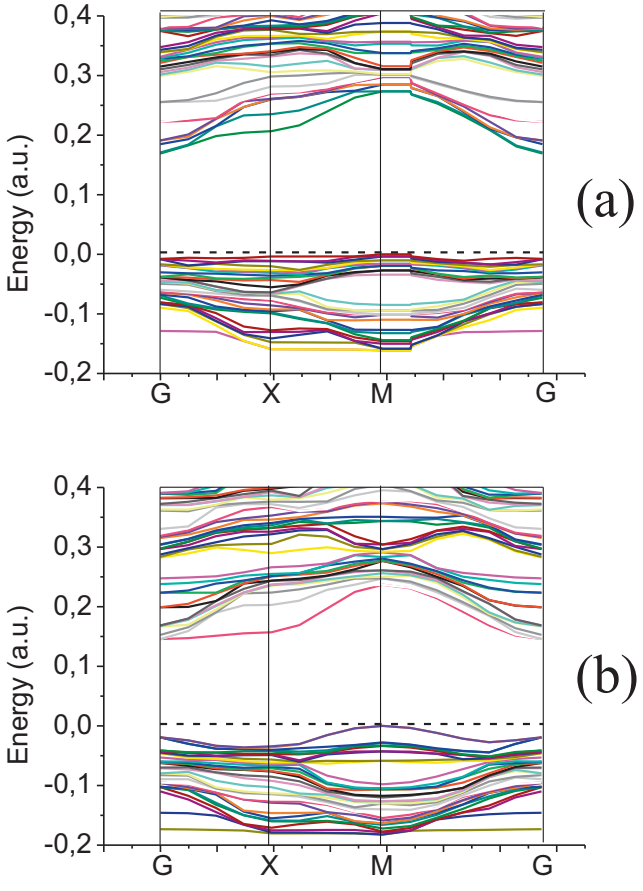

Fig. 8 Our B3PW calculated electronic band structure for $BaZrO_3$ BaO (a) and ZrO_2-terminated (b) (001) surfaces.

0.098*e*. B3PW and B3LYP calculated B–O chemical bond populations near the ABO_3 perovskite (001) surfaces are in the range from 0.102*e* for the $CaZrO_3$ (001) surface case till 0.132*e* for the $BaZrO_3$ perovskite (001) surface. The (001) surface B–O chemical bond population coincides for all three $PbTiO_3$, $CaTiO_3$ and $SrZrO_3$ perovskite (001) surfaces and are equal to 0.114*e*. The (011) surface B–O chemical bond populations are even larger than the respective chemical bond populations for the (001) surface, and are in the range from 0.128*e* for the $CaTiO_3$ (011) surface case, to 0.152*e* for the $BaZrO_3$ perovskite (011) surface. The systematic trend for all calculated ABO_3 perovskites is that the B–O chemical bond populations are larger near the (011) surface, than near the (001) surface, and the B–O chemical bond populations in the ABO_3 perovskite bulk always are smaller than near their (001) and, of course, (011) surfaces. For example, for the $BaZrO_3$ perovskite bulk, the Zr–O chemical bond population is equal to 0.108*e*. The Zr–O chemical bond population becomes larger near the ZrO_2-terminated $BaZrO_3$ (001)

Table 8 B3PW and B3LYP calculated B–O chemical bond populations for $SrTiO_3$, $BaTiO_3$, $PbTiO_3$, $CaTiO_3$, $SrZrO_3$, $BaZrO_3$, $PbZrO_3$ and $CaZrO_3$ bulk as well as for BO_2-terminated (0 0 1) and BO-terminated (0 1 1) surfaces (in *e*).

Material	Method	B–O chemical bond population		
		Bulk	(0 0 1) surface	(0 1 1) surface
$SrTiO_3$ [20]	B3PW	0.088	0.118	0.130
$BaTiO_3$ [19]	B3PW	0.098	0.126	0.130
$PbTiO_3$ [19]	B3PW	0.098	0.114	0.132
$CaTiO_3$ [18]	B3PW	0.084	0.114	0.128
$SrZrO_3$ [29]	B3LYP	0.092	0.114	0.142
$BaZrO_3$ [32]	B3PW	0.108	0.132	0.152
$PbZrO_3$ [29]	B3LYP	0.106	0.116	0.148
$CaZrO_3$ [38]	B3LYP	0.086	0.102	

surface 0.132*e*, and it reaches the largest value of 0.152*e* near the ZrO-terminated $BaZrO_3$ (0 1 1) surface.

4. Summary and conclusions

Based on the large amount of our B3PW and B3LYP calculations, performed for ABO_3 perovskite (0 0 1) surfaces, following systematic trends were detected:

1. The relaxation of (0 0 1) surface metal atoms for ABO_3 perovskite upper two surface layers for both AO and BO_2-terminations, in most cases, are considerably larger than that of oxygen atoms, what leads to a considerable rumpling of the outermost plane.
2. For the AO and BO_2-terminated (0 0 1) surfaces of ABO_3 perovskites, the systematic trend, with a few exceptions, according to performed B3PW and B3LYP calculations, is that all atoms of the first surface layer relax inward, all atoms of the second surface layer relax outward, and all atoms of the third surface layer, again, relax inward. As a result of this relaxation, our calculated surfaces exhibit the reduction of the interlayer distance Δd_{12} and expansion of Δd_{23}.
3. For all eight B3PW and B3LYP calculated ABO_3 perovskites, the changes in interlayer distances Δd_{12} are larger than the respective changes in the interlayer distances Δd_{23}.
4. The ABO_3 perovskite (0 0 1) surface energies for both AO and BO_2-terminations are almost equal. In contrast (0 1 1) and especially (1 1 1) surface energies for different terminations, in most cases, are quite different.
5. The ABO_3 perovskite (0 0 1) surface energies always are smaller than the (0 1 1) and especially (1 1 1) surface energies.
6. According to our performed B3PW, B3LYP, PWGGA and HF calculations, the ABO_3 perovskite AO and BO_2-terminated (0 0 1) surface band gaps are always reduced with respect to their bulk band gap values. The only exception, to the best of our knowledge, is the paper by Meyer et al. [58], where the LDA calculated band gaps for SrO-terminated $SrTiO_3$ (1.86 eV), BaO-terminated $BaTiO_3$ (1.80 eV) as well as TiO_2-terminated $PbTiO_3$ (1.61 eV) (0 0 1) surfaces are larger than the respective $SrTiO_3$ (1.85 eV), $BaTiO_3$ (1.79 eV) and $PbTiO_3$ (1.54 eV) bulk band gaps. Nevertheless, the bulk and surface band gap values presented in Ref. [58] are very close, and thereby they are practically in the precision limit of calculations, and cannot rigorously refute our conclusion, that the ABO_3 perovskite (0 0 1) surface band gaps are always reduced with respect to the bulk band gap values.
7. The B–O chemical bond population in ABO_3 perovskite bulk always are smaller than near the (0 0 1) and especially (0 1 1) surfaces.

Acknowledgements

This work was supported by the Latvian Council of Science Grant No. 374/2012 and the Latvian National Research Program IMIS2. Many stimulating discussions with D. Vanderbilt, K.M. Rabe, M. Rohlfing, E. Heifets, J. Maier, G. Borstel and E.A. Kotomin are greatly acknowledged.

References

[1] L. Kronik, Y. Shapira, Surf. Sci. Rep. 37 (1999) 1–206.
[2] A. Weizman, D. Fuks, E.A. Kotomin, D. Gryaznov, Solid State Ionics 230 (2013) 32–36.
[3] M.M. Kuklja, Y.A. Mastrikov, B. Jansang, E.A. Kotomin, Solid State Ionics 230 (2013) 21–26.
[4] C. Lushchik, E. Feldbach, A. Frorip, M. Kirm, A. Lushchik, A. Maaroos, I. Martinson, J. Phys.: Condens. Matter 6 (1994) 11177.
[5] R. Yukawa, K. Ozawa, S. Yamamoto, R.Y. Liu, I. Matsuda, Surf. Sci. 641 (2015) 224–230.
[6] B.G. Janesko, S.I. Jones, Surf. Sci. 659 (2017) 9–15.
[7] S.N. Vidhya, O.N. Balasundaram, M. Chandramohan, J. Saudi Chem. Soc. 20 (2016) 703–710.
[8] A. Irfan, A.G. Al-Sehemi, S. Muhammad, A.R. Chaudhry, A. Kalam, M. Shkir, A.E. AL-Salami, A.M. Asiri, J. Saudi Chem. Soc. 20 (2016) 680–685.
[9] M.R. Belkhedkar, A.U. Ubale, J. Saudi Chem. Soc. 20 (2016) 553–560.
[10] V. Dimza, A.I. Popov, L. Lace, M. Kundzins, K. Kundzins, M. Antonova, M. Livins, Curr. Appl. Phys. 17 (2017) 169–173.
[11] S. Min, X. Yang, A. Lu, C. Tseng, M.N. Hedhili, Z. Lai, L. Li, K. Huang, J. Saudi Chem. Soc. 21 (2017) 708–712.
[12] Yu.F. Zhukovskii, N. Pugno, A.I. Popov, C. Balasubramanian, S. Bellucci, J. Phys.: Condens. Matter 19 (2007) 395021.
[13] M. Haghighi, K. Nikoofar, J. Saudi Chem. Soc. 20 (2016) 101–106.
[14] A.U. Ubale, M.V. Bhute, G.P. Malpe, P.R. Raut, K.S. Chipade, S.G. Ibrahim, J. Saudi Chem. Soc. 20 (2016) 227–236.

[15] L. Miao, R. Jia, Y. Wang, C.-P. Kong, J. Wang, R.I. Eglitis, H.-X. Zhang, J. Saudi Chem. Soc. 21 (2017) 111–117.
[16] H.Y. Hwang, Y. Iwasa, M. Kawasaki, B. Keimer, N. Nagaosa, Y. Tokura, Nat. Mater. 11 (2012) 103–113.
[17] T. Matsuda, S. Yamanaka, K. Kurosaki, S.I. Kobayashi, J. Alloys. Compd. 351 (2003) 43–46.
[18] R.I. Eglitis, D. Vanderbilt, Phys. Rev. B 78 (2008) 155420.
[19] R.I. Eglitis, D. Vanderbilt, Phys. Rev. B 76 (2007) 155439.
[20] R.I. Eglitis, D. Vanderbilt, Phys. Rev. B 77 (2008) 195408.
[21] M. Dawber, K.M. Rabe, J.F. Scott, Rev. Mod. Phys. 77 (2005) 1083–1130.
[22] N. Erdman, K.R. Poeppelmeier, M. Asta, O. Warschkow, D.E. Ellis, L.D. Marks, Nature 419 (2002) (2002) 55–58.
[23] E. Heifets, R.I. Eglitis, E.A. Kotomin, J. Maier, G. Borstel, Phys. Rev. B 64 (2001) 235417.
[24] J.M.P. Martirez, E.H. Morales, W.A. Saidi, D.A. Bonnell, A.M. Rappe, Phys. Rev. Lett. 109 (2012) 256802.
[25] J.M. Zhang, Q. Pang, K.W. Hu, V. Ji, Surf. Interface Anal. 40 (2008) 1382–1387.
[26] G.Z. Wang, C.R. Li, J. Cui, Z.Y. Man, Surf. Interface Anal. 41 (2009) 918–923.
[27] J.R. Sambrano, V.M. Longo, E. Longo, C.A. Taft, J. Mol. Struct. (Thoechem) 813 (2007) 49–56.
[28] H. Tian, A.J. Mao, H.J. Zhao, Y. Cui, H. Li, X.Y. Kuang, Phys. Chem. Chem. Phys. 18 (2016) 7680–7687.
[29] R.I. Eglitis, M. Rohlfing, J. Phys.: Condens. Matter 22 (2010) 415901.
[30] R.I. Eglitis, S. Piskunov, Comput. Condens. Matter 7 (2016) 1–6.
[31] M. Arrigoni, T.S. Bjørnheim, E.A. Kotomin, J. Maier, Phys. Chem. Chem. Phys. 18 (2016) 9902–9908.
[32] R.I. Eglitis, J. Phys.: Condens. Matter 19 (2007) 356004.
[33] Y.X. Wang, M. Arai, T. Sasaki, C.L. Wang, W.L. Zhong, Surf. Sci. 585 (2005) 75–84.
[34] R.I. Eglitis, Int. J. Mod. Phys. B 28 (2014) 1430009.
[35] S. Piskunov, R.I. Eglitis, Solid State Ionics 274 (2015) 29–33.
[36] S. Piskunov, R.I. Eglitis, Nucl. Instr. Methods Phys. Res. B 374 (2016) 20–23.
[37] M.G. Brik, C.G. Ma, V. Krasnenko, Surf. Sci. 608 (2013) 146–153.
[38] R.I. Eglitis, Ferroelectrics 483 (2015) 75–85.
[39] A. Biswas, P.B. Rossen, C.H. Yang, W. Siemons, M.H. Jung, I. K. Yang, R. Ramesh, Y.H. Jeong, Appl. Phys. Lett. 98 (2011) 051904.
[40] G.Z. Zhu, G. Radtke, G.A. Botton, Nature 490 (2012) 384–387.
[41] R. Shimizu, K. Iwaya, T. Ohsawa, S. Shiraki, T. Hasegawa, T. Hashizume, T. Hitosugi, Appl. Phys. Lett. 100 (2012) 263106.
[42] T. Kubo, H. Orita, H. Nozoye, Phys. Chem. Chem. Phys. 13 (2011) 16516–16519.
[43] M.S.J. Marshall, D.T. Newell, D.J. Payne, R.G. Egdell, M.R. Castell, Phys. Rev. B 83 (2011) 035410.
[44] R. Courths, Phys. Stat. Sol. B 100 (1980) 135–148.
[45] T. Shimizu, H. Bando, Y. Aiura, Y. Haruyama, K. Oka, Y. Nishihara, Jpn. J. Appl. Phys. 34 (1995) L1305–L1308.
[46] N. Bickel, G. Schmidt, K. Heinz, K. Muller, Phys. Rev. Lett. 62 (1989) 2009–2011.
[47] T. Hikita, T. Hanada, M. Kudo, M. Kawai, Surf. Sci. 287–288 (1993) 377–381.
[48] J.W. Edwards, R. Speiser, H.L. Johnston, J. Amer. Chem. Soc. 73 (1951) 2934–2935.
[49] K. van Benthem, C. Elsässer, R.H. French, J. Appl. Phys. 90 (2001) 6156–6164.
[50] S.H. Wemple, Phys. Rev. B 2 (1970) 2679–2689.
[51] J.G. Bednorz, H.J. Scheel, J. Cryst. Growth 41 (1977) 5.
[52] S.A. Mabud, A.M. Glazer, J. Appl. Cryst. 12 (1979) 49–53.
[53] H. Fujishita, S. Hoshino, J. Phys. Soc. Jpn. 53 (1984) 226–234.
[54] R.J. Nelmes, W.F. Kuhs, Solid State Commun. 54 (1985) 721–723.
[55] M. Sato, Y. Soejima, N. Ohama, A. Okazaki, H.J. Scheel, K.A. Müller, Phase Trans. 5 (1985) 207–218.
[56] M.D. Mathews, E.B. Mirza, A.C. Momin, J. Mater. Sci. Lett. 10 (1991) 305–306.
[57] Y. Du, Z.P. Jin, P.Y. Huang, J. Am. Ceram. Soc. 75 (1992) 3040.
[58] B. Meyer, J. Padilla, D. Vanderbilt, Faraday Discuss. 114 (1999) 395–405.
[59] B.J. Kennedy, C.J. Howard, B.C. Chakoumakos, Phys. Rev. B 59 (1999) 402.
[60] J. Robertson, J. Vacuum Sci. Technol. B 18 (2000) 1785–1791.
[61] S. Aoyagi, Y. Kuroiwa, A. Sawada, H. Tanaka, E. Nishibori, M. Takata, M. Sakata, J. Phys. Soc. Japan 71 (2002) 2353–2356.
[62] R. Ali, M. Yashima, J. Solid State Chem. 178 (2005) 2867.
[63] M. Yoshino, H. Yukawa, M. Morinaga, Mater. Trans. 45 (2004) 2056–2061.
[64] P. Stoch, J. Szczerba, J. Lis, D. Madej, Z. Peogonekdzich, J. Eur. Ceram. Soc. 32 (2012) 665–670.
[65] I.L.V. Rosa, M.C. Oliveira, M. Assis, M. Ferrer, R.S. André, E. Longo, M.F.C. Gurgel, Ceram. Int. 41 (2015) 3069–3074.
[66] C.H. Peng, J.F. Chang, S. Desu, Mater. Res. Soc. Symp. Proc. 243 (1992) 21–24.
[67] K. Ueda, H. Yanagi, R. Noshiro, H. Hosono, H. Kawazoe, J. Phys.: Condens. Matter 10 (1998) 3669–3677.
[68] Y.S. Lee, J.S. Lee, T.W. Noh, D.Y. Byun, K.S. Yoo, K. Yamaura, E. Takayama-Muromachi, Phys. Rev. B 67 (2003).
[69] R.I. Eglitis, Solid State Ionics 230 (2013) 43–47.
[70] N. Sivadas, H. Dixit, V.R. Cooper, D. Xiao, Phys. Rev. B 89 (2014) 075303.
[71] R.I. Eglitis, Appl. Surf. Sci. 358 (2015) 556–562.
[72] H. Chen, Y. Xie, G.X. Zhang, H.T. Yu, J. Phys.: Condens. Matter 26 (2014) 395002.
[73] R.I. Eglitis, Phys. State Sol. B 252 (2015) 635–642.
[74] S. Piskunov, E. Heifets, R.I. Eglitis, G. Borstel, Comput. Mater. Sci. 29 (2004) 165–178.
[75] A.D. Becke, J. Chem. Phys. 98 (1993) 5648–5652.
[76] C. Lee, W. Yang, R.G. Parr, Phys. Rev. B 37 (1988) 785–789.
[77] V.R. Saunders, R. Dovesi, C. Roetti, N. Causa, N.M. Harrison, R. Orlando, C.M. Zicovich-Wilson, CRYSTAL-2009 User Manual University of Torino Italy, 2009.
[78] H.J. Monkhorst, J.D. Pack, Phys. Rev. B 13 (1976) 5188–5192.
[79] R.C. Bochicchio, H.F. Reale, J. Phys. B 26 (1993) 4871–4883.
[80] K.H. Hellwege, A.M. Hellwege, Landolt-Bornstein New Series, Springer, Berlin, 1969. p. 3.
[81] R.S. Roth, J. Res. Natl. Bureau Stand. 58 (1957) 75–88.
[82] Y.X. Wang, M. Arai, T. Sasaki, C.L. Wang, Phys. Rev. B 73 (2006) 035411.
[83] Y.X. Wang, M. Arai, Surf. Sci. 601 (2007) 4092.

Institute of Solid State Physics, University of Latvia as the Center of Excellence has received funding from the European Union's Horizon 2020 Framework Programme H2020-WIDESPREAD-01-2016-2017-TeamingPhase2 under grant agreement No. 739508, project CAMART²